Metabolic Engineering 82 (2024) 262–273

Contents lists available at ScienceDirect

Metabolic Engineering

journal homepage: www.elsevier.com/locate/meteng

Metabolic flux optimization of iterative pathways through orthogonal gene expression control: Application to the β-oxidation reversal

Seung Hwan Lee [1], Yang Hu [1], Alexander Chou, Jing Chen, Ramon Gonzalez [*]

Department of Chemical, Biological, and Materials Engineering, University of South Florida, Tampa, FL, USA

ARTICLE INFO

Keywords:
Iterative metabolic pathways
Combinatorial Biosynthesis
Orthogonal control of gene expression
RBOX
TriO

ABSTRACT

Balancing relative expression of pathway genes to minimize flux bottlenecks and metabolic burden is one of the key challenges in metabolic engineering. This is especially relevant for iterative pathways, such as reverse β-oxidation (rBOX) pathway, which require control of flux partition at multiple nodes to achieve efficient synthesis of target products. Here, we develop a plasmid-based inducible system for orthogonal control of gene expression (referred to as the TriO system) and demonstrate its utility in the rBOX pathway. Leveraging effortless construction of TriO vectors in a plug-and-play manner, we simultaneously explored the solution space for enzyme choice and relative expression levels. Remarkably, varying individual expression levels led to substantial change in product specificity ranging from no production to optimal performance of about 90% of the theoretical yield of the desired products. We obtained titers of 6.3 g/L butyrate, 2.2 g/L butanol and 4.0 g/L hexanoate from glycerol in *E. coli*, which exceed the best titers previously reported using equivalent enzyme combinations. Since a similar system behavior was observed with alternative termination routes and higher-order iterations, we envision our approach to be broadly applicable to other iterative pathways besides the rBOX. Considering that high throughput, automated strain construction using combinatorial promoter and RBS libraries remain out of reach for many researchers, especially in academia, tools like the TriO system could democratize the testing and evaluation of pathway designs by reducing cost, time and infrastructure requirements.

1. Introduction

One of the key challenges in the engineering and optimization of metabolic pathways is the imbalance of metabolic fluxes leading to bottlenecks and undesired byproduct formation (Stephanopoulos et al., 1998). At large, flux debottlenecking can be accomplished by: (1) employing pathway enzymes with the proper catalytic efficiency and substrate specificity; and (2) fine-tuning the relative concentrations of said enzymes (Lee et al., 2013, 2023). Kinetic properties greatly affect the pathway flux and advanced tools in genome mining and protein engineering can be leveraged to ensure the use of proper enzymes (Lee et al., 2023). However, even catalytically efficient enzymes expressed at high levels often lead to suboptimal operation and cause metabolic burdens. Current metabolic engineering strategies often rely on gene expression from a constitutive promoter or a single inducible promoter that does not allow independent control of relative expression of multiple pathway enzymes. While recent developments in promoter (Fleur et al., 2021) and RBS (Reis and Salis, 2020) engineering allow individual gene regulation via genetic modifications, its use in optimizing relative gene expression often requires construction of promoter and/or RBS libraries followed by extensive screening (Park et al., 2023). Moreover, such approaches relying on constitutive expression could exert metabolic burden at exponential growth phase resulting in decreased enzyme expression levels and lower product titer (Ni et al., 2021). Alternatively, gene expression could be controlled *in situ* through dynamic gene expression control systems (Ni et al., 2021). These systems can be regulated by various sensors such as temperature (Harder et al., 2018), light (Zhao et al., 2018), pH (Yin et al., 2017) and small molecules (Meyer et al., 2019). Among them, orthogonal inducible promoters to independently regulate individual gene expression is particularly relevant for the goal of optimizing relative gene expressions in metabolic pathways consisting of multiple enzymes.

Optimization of relative gene expression levels becomes particularly important in iterative pathways, where a small set of core elongation enzymes catalyze the same biochemistries in a repetitive fashion using substrates of different chain lengths. Therefore, these core enzymes must be promiscuous and exhibit broad change-length specificities towards their substrates, otherwise a different set of enzymes would be needed

* Corresponding author.ramongonzale@usf.edu
[1] These authors contributed equally: Seung Hwan Lee, Yang Hu.

https://doi.org/10.1016/j.ymben.2024.02.007
Received 27 August 2023; Received in revised form 2 February 2024; Accepted 13 February 2024
Available online 20 February 2024

for each iteration of the pathway. Unfortunately, this enzyme promiscuity often leads to the synthesis of product mixtures as opposed to the desired pure, single product. Byproduct formation and yield loss could be further exacerbated by the accumulation of pathway intermediates, often resulting from imbalance between substrate and enzyme concentrations (Ni et al., 2021). We hypothesized that such limitations could be overcome by finetuning relative expression levels of individual pathway enzymes, thereby creating optimal metabolic flux streamlining entry to desired product in the iterative pathways. As a testbed for this system, we decided to use the reverse β-oxidation (rBOX) cycle (Fig. 1), which has previously been implemented only with a single inducible promoter system (Clomburg et al., 2012; Dellomonaco et al., 2011). The rBOX pathways allow efficient production of alcohols and acids with various chain lengths and functionalities through iterations of priming and elongation steps, followed by termination at specific nodes (Cheong et al., 2016; Clomburg et al., 2015; Kim et al., 2015; Tan et al., 2020; Tarasava et al., 2022). A recent study demonstrates relative protein levels in rBOX pathway are crucial in determining product profile and titer (Courtney et al., 2023) *in vitro*, but this phenomenon has yet to be demonstrated *in vivo*.

Exploration of the two-parameter solution space comprising enzyme selection and enzyme expression can quickly become impractical, especially for pathways consisting of multiple reaction steps. While advances in scale-down and automation of strain construction as well as decreasing costs of DNA synthesis have made combinatorial approaches more accessible, these methods remain out of reach for many researchers especially in academia (Park et al., 2023). To address this, we developed a plasmid-based orthogonal gene expression system to enable independent control of 3 different operons *in vivo* (and more when used in combination with other systems), which we refer to as the TriO system. This work builds upon the previously developed orthogonal inducible transcription machinery, known as the "Marionette" system (Meyer et al., 2019). Combinatorial optimization of relative expression levels of pathway enzymes allowed substantial debottlenecking of the rBOX pathway and resulted in significant improvement in titers, rates and yields of rBOX products in different functional groups and chain lengths. Moreover, parallel investigation of enzyme selection and expression revealed the previously unidentified tradeoff between efficiency and stability in the enzyme choice for the pathway.

2. Results

2.1. Construction and characterization of the TriO vector system

The TriO vectors were designed to enable the exploration of the largest pathway solution space possible with a minimal amount of strain construction and cloning. To this end, a plasmid-based system was envisioned for convenience. Plasmids can be rapidly constructed,

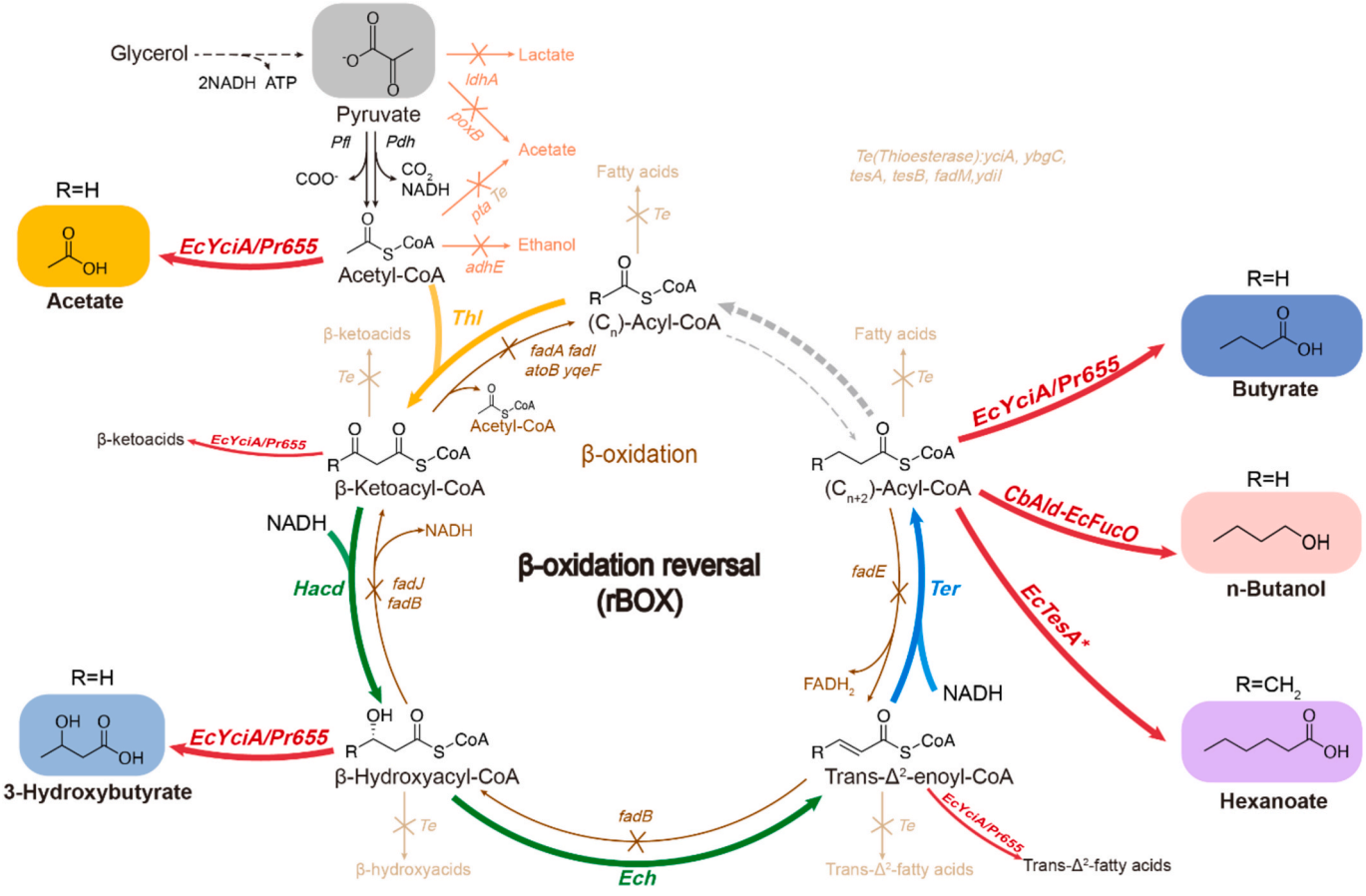

Fig. 1. Reverse β-oxidation (rBOX) pathway for butyrate, n-butanol, and hexanoate production in FTBOX host. FTBOX strain represents an engineered variant of *E. coli* strain MG1655 (DE3), deficient in fermentation, thioesterase, and beta-oxidation pathways. The orange crossed lines indicate the deletion of native fermentative pathways (Δ*ldhA* Δ*poxB* Δ*pta* Δ*adhE* Δ*frdA*). The tan crossed lines indicate the deletion of the native thioesterases (Δ*yciA*, Δ*ybgC*, Δ*tesA*, Δ*tesB*, Δ*fadM*, and Δ*ydiI*). The brown crossed lines represent the deletion of the native β-oxidation pathway (Δ*fadBA*, Δ*fadJI*, Δ*atoB*, and Δ*yqeF*). Major products observed in the extracellular media are highlighted in bold with colored boxes. Bold solid arrows of different colors represent rBOX enzymes expressed under four orthogonal inducible promoters. Thl: 3-ketoacyl-CoA thiolase; Hacd: 3-hydroxyacyl-CoA dehydrogenase; Ech: enoyl-CoA hydratase; Ter: transenoyl-CoA reductase; Te: acyl-CoA thioesterase; ldhA: lactate dehydrogenase; poxB: pyruvate oxidase; adhE: acyl-CoA reductase-alcohol dehydrogenase; pta: phosphoacetyltransferase; Pfl: pyruvate formate lyase; Pdh: pyruvate dehydrogenase complex.

maintained, and sequence-verified using well-established methods with low cost, and they can be readily implemented in different host chassis. Moreover, plasmid-based systems also provide an additional point of gene expression control by manipulating the number of copies through varying the origin of replication. While the cost of the antibiotics and long-term stability become the concern under industrial settings, measures to address these drawbacks, such as plasmid addiction systems (Kroll et al., 2010) have been demonstrated for stable product synthesis under extended timeframe with no antibiotics requirement (Laguna et al., 2015).

We designed a cloning strategy that maximizes the ability to assemble various gene candidates in a combinatorial manner (Fig. 2A). First, we constructed individual vectors, named "entry vectors", each with transcription units comprised of one of three independent inducible promoters controlled by cuminic acid (cumate), 2,4-diacetylphophloroglucinol (DAPG) or vanillic acid (vanillate), a strong RBS, a cloning site, and a terminator sequence. Genes encoding the enzymes of interest can be inserted into the entry vectors in the same way as other common plasmids, for example by Gibson Assembly or restriction enzyme digestion and ligation. We further constructed "destination vectors" which harbor an operon for constitutive expression of the repressors for each inducible promoter (CymR, PhlF, and VanR for cumate, DAPG and vanillate, respectively). We used pACYCDuet-1(Novagen) as the backbone, which carries the P15A replicon and the chloramphenicol resistance gene, and ultimately formed the pACYC3 destination vector. The three entry vectors (pCEntry: cumate, pPEntry: DAPG, and pVEntry: vanillate) and the destination vectors (pACYC3) can be assembled into the final vector, named the "TriO" vector, via one-step Golden Gate Assembly (Fig. 2A). This approach, which draws inspiration from MoClo-based strategies (Peccoud et al., 2011), allows for sequence verified entry vectors to be stocked and the various transcription units to be assembled in a combinatorial manner as needed. The laborious cloning steps therefore need to be undertaken only once, after which expression of the enzymes can be implemented in different combinations and at different levels.

We utilized the expression of fluorescent proteins to validate the design and functionality of the TriO vector system. The genes encoding eYFP, mRFP1, and eGFP were inserted into the pCEntry, pPEntry, and

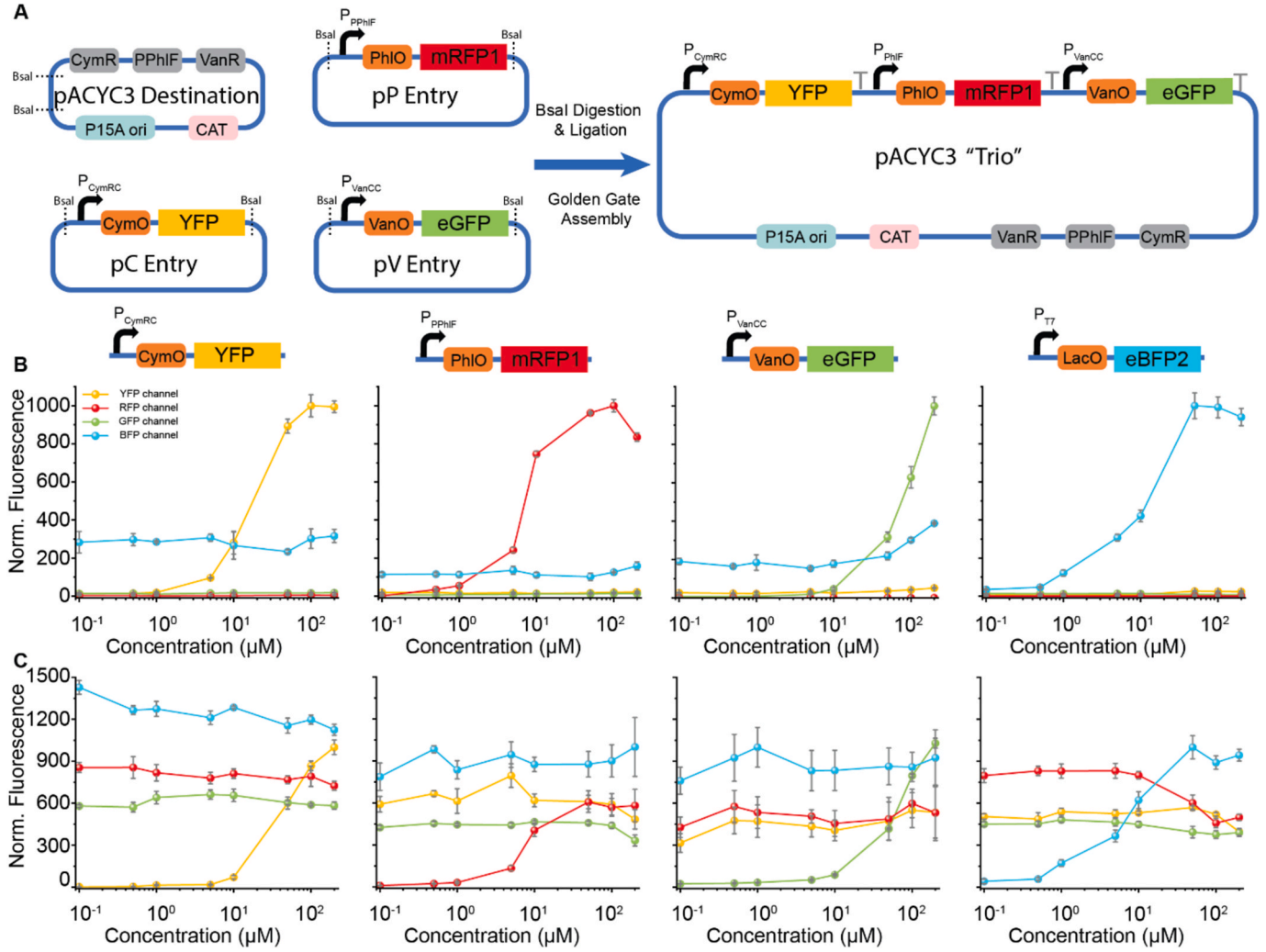

Fig. 2. Trio vector construction and validation. (A) Construction of TriO vector using one-step Golden Gate assembly of three entry vectors carrying genes under orthogonal inducible promoters and the destination vector (pACYC3). pCEntry harbors a cumate-inducible CymRC promoter; pPEntry harbors a DAPG-inducible PhlF promoter; and pVEntry harbors a vanillate-inducible VanCC promoter. (B) Validation of independency of individual gene expression using fluorescent proteins. Cumate-inducible yellow fluorescent protein (YFP), DAPG-inducible red fluorescent protein (RFP), vanillate-inducible green fluorescent protein (eGFP) and IPTG-inducible blue fluorescent protein (eBFP2) are orthogonally expressed in response to varying concentrations of each individual inducer. (C) Validation of orthogonality of TriO vector in the presence of other inducers: each inducible promoter was tested in the presence of 0.1 mM of other 3 inducers (e.g., cumate induction was tested in the presence of 0.1 mM DAPG, 0.1 mM vanillate and 0.1 mM IPTG). Dots are drawn to the mean values with error bars indicating the standard deviation of biological triplicates.

pVEntry vectors, respectively. The TriO expression vector was assembled using the pACYC3 destination vector (Fig. 2A). To verify its compatibility with commonly used IPTG-inducible promoters (such as the trc and T7lac promoter systems), we placed eBFP2 in the P1 site of the standard pCDFDuet-1 vector (Novagen). *E. coli* MG1655 (DE3) strain harboring the assembled vector was grown in the presence of varying concentrations of cumate, DAPG, vanillate and IPTG to induce expression of eYFP, mRFP1, eGFP and eBFP2, respectively. We found that a linear vertical and exponential horizontal plot better demonstrated the relationship between different concentrations of inducers and the fluorescence of the expressed proteins (Fig. S2). As illustrated in Fig. 2B, the addition of inducers resulted in the dose-dependent expression of the relevant fluorescent proteins. Additionally, none of the inducers affected expression of other fluorescent proteins significantly, indicating that the transcriptional units were well insulated.

To test the orthogonality of the TriO vector in the presence of other inducers, we examined the expression of eYFP, mRFP1, eGFP, and eBFP2 under various concentrations of cumate, DAPG, vanillate, and IPTG with three other inducible promoters at high expression levels (0.1 mM) (Fig. 2C). A comparison between Fig. 2B and C reveals a consistent trend in the expression of fluorescent proteins with different concentrations of inducers, with minimal interference from other inducers. These results demonstrate that the TriO vector, in combination with pCDFDuet-1, forms a four-control-point orthogonal gene induction system, where each inducer independently regulates the expression levels.

2.2. Reconstruction of one-turn rBOX pathway using the TriO vector

We initially used TriO vector to implement the one-turn rBOX pathway producing butyric acid (butyrate). A previous study (Clomburg et al., 2012) used a single inducible promoter system (P_{trc}) to express AtoB (thiolase, Thl) and FadB (hydroxyacyl-CoA dehydrogenase, Hacd, and enoyl-CoA hydratase, Ech) from *E. coli* and EgTER (enoyl-CoA reductase, Ter) from *Euglena gracilis* (Fig. 1). Subsequently, a TriO vector harboring cumate-inducible *atoB*, DAPG-inducible *egTER* and vanillate-inducible *fadB* was constructed (Fig. 3). To investigate the impact of relative gene expression, three inducer levels (high, medium, and low) from each promoter were used based on the results from fluorescent protein assays (Fig. 2B). These inducer levels were then arranged in a full factorial, which makes up 27 different combinations of inducer concentrations (Fig. S1). Based on the fermentation results, butyrate production ranged from 0.1 g/L to 0.9 g/L, which shows the importance of relative gene expressions in the product synthesis. These experiments also demonstrate that finetuning of expression levels is necessary to achieve optimal pathway performance.

2.3. Host engineering to minimize crosstalk between rBOX and native metabolic pathways

For initial testing of the TriO vector, we utilized strain JC01, which is devoid of fermentative pathways (*ΔldhA ΔpoxB Δpta ΔadhE ΔfrdA*) (Clomburg et al., 2012; Dellomonaco et al., 2011) to minimize the formation of byproducts (lactate, ethanol and acetate) that compete with the rBOX for precursor metabolites (pyruvate and acetyl-CoA) and reducing equivalents (NADH) (Fig. 1). A follow up study (Kim et al., 2015) demonstrated that knocking out six native thioesterases (*yciA*, *ybgC*, *tesA*, *tesB*, *fadM* and *ydiI*) significantly improves the yield and titer of medium-chain (C6–C10) rBOX products by preventing the undesired hydrolysis of CoA thioesters acting as primers, extenders, and intermediates in the rBOX pathway. This strain harboring λDE3 lysogen for chromosomal T7 RNA polymerase expression and having an additional deletion of the gene encoding acyl-CoA dehydrogenase (*fadE*) was named JST07 (DE3) and used to generate various rBOX products (Cheong et al., 2016; Clomburg et al., 2015; Kim et al., 2015; Kim and Gonzalez, 2018) (Fig. 1). In the context of this study, it is also important to finetune individual gene expression and avoid any background

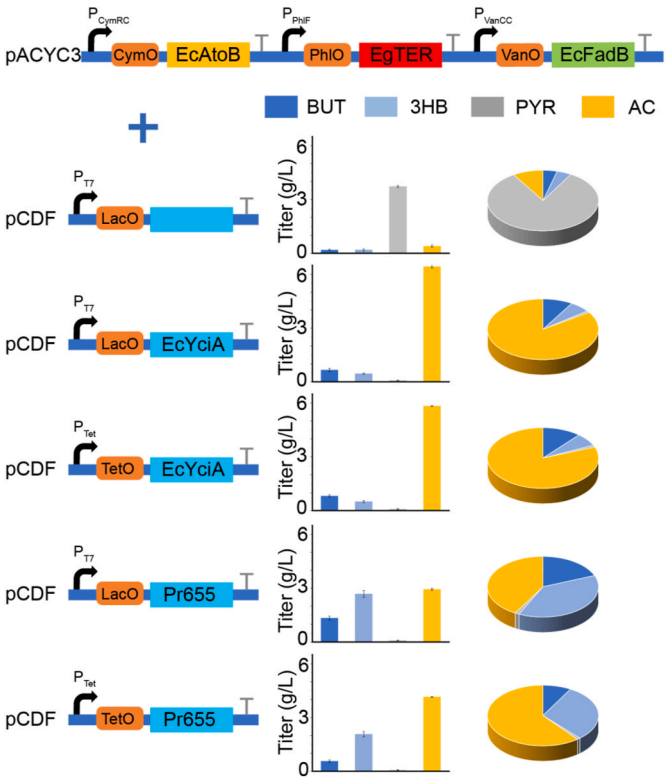

Fig. 3. Investigation of termination enzymes for one-turn rBOX cycle. Metabolite profiles of strain FTBOX harboring the TriO vector with cumate-inducible EcAtoB, DAPG-inducible EgTER, and vanillate-inducible EcFadB with empty pCDFDuet-1 vector, IPTG-inducible EcYciA, aTc (anhydrotetracycline)-inducible EcYciA, IPTG-inducible Pr655 or aTc-inducible Pr655. Bars are drawn to the mean values with error bars indicating the standard deviation of biological triplicates. BUT: butyrate; 3HB: 3-hydroxybutyrate; PYR: pyruvate; AC: acetate.

from/crosstalk with native enzymes. To achieve this, we deleted all known native β-oxidation genes (*fadBA, fadJI, atoB and yqeF*) from JST07 (DE3) to make it a fermentation-, thioesterase-, and beta-oxidation-deficient strain, which was named as FTBOX strain (Fig. 1 and Table S1). The FTBOX chassis minimizes fermentative byproduct synthesis, undesired hydrolysis of rBOX primers, extenders, and intermediates, and prevents native β-oxidation enzymes from competing with rBOX enzymes expressed via the TriO vector (Fig. 1).

2.4. Controlled thioesterase expression with TriO vector for butyrate production

Previous studies on butyrate production from rBOX relied on endogenous "background" thioesterase activity of the host JC01 while the overexpression of an active thioesterase, *yciA*, under inducible promoter resulted in significant decrease in butyrate titer and acetate accumulation (Clomburg et al., 2012). We hypothesized that although YciA has approximately 10-fold higher specific activity with butyryl-CoA than with acetyl-CoA, the abundance of acetyl-CoA in the cell caused premature hydrolysis to acetate causing significant drop in the rBOX products (Clomburg et al., 2012). Finding an enzyme that is more specific toward butyryl-CoA (i.e., lower promiscuous activity with acetyl-CoA) would be a possible solution to address this. Alternatively, it could be feasible to finetune the flux from acetyl-CoA between the condensation (thiolase) and the hydrolysis (thioesterase) by manipulating enzyme expression levels.

To investigate whether we can address the undesired hydrolysis by independently controlling the expression of thioesterase and rBOX genes, the TriO vector harboring rBOX genes (*atoB*, *fadB* and *egTER*) and

pCDFDuet-1 harboring *E. coli yciA* (pCDFDuet-P1-*yciA*) were transformed into strain FTBOX (Fig. 3). Cumate, DAPG and vanillate concentrations for the TriO vector were set at the same level as the best condition observed from JC01 control with 3 × 3 × 3 full factorial (Fig. S1 and 5 μM cumate, 10 μM DAPG and 10 μM vanillate). The control strain harboring empty pCDFDuet-1 vector produced primarily pyruvate with minimal rBOX products (Fig. 3). This result indicates successful deletion of native thioesterases that have a major role in hydrolyzing intermediate and product acyl-CoAs. The absence of a termination enzyme likely caused a bottleneck downstream of pyruvate node in the rBOX pathway, where intermediate acyl-CoA molecules cannot be transported intermembrane of the cells. A small amount of acetate is potentially due to spontaneous hydrolysis of acetyl-CoA and weak activities of endogenous thioesterase other than the six already deleted. Interestingly, introduction of *yciA* dramatically shifted the production to acetate, even when there is no IPTG addition (Fig. 3). This indicates that the leaky expression of YciA under the T7lac promoter is enough to hydrolyze most acetyl-CoA before it enters the rBOX. To

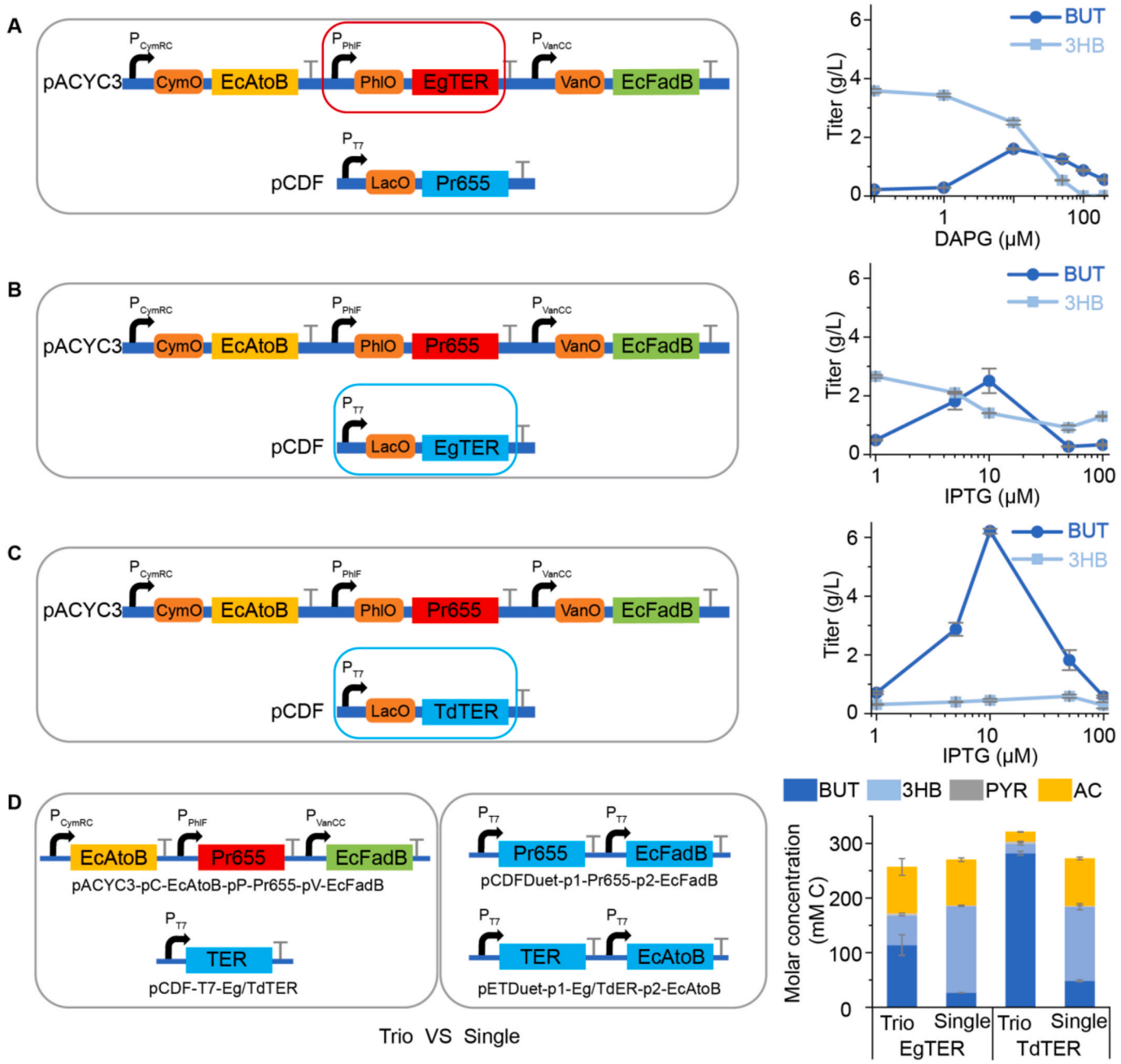

Fig. 4. Debottlenecking one-turn rBOX via enzyme selection and expression level optimization of enoyl-CoA reductase (Ter). Production of butyrate (BUT) and 3-hydroxybutyrate (3HB) by strain FTBOX harboring (A) DAPG-inducible EgTER and IPTG-inducible Pr655 at varying levels of DAPG concentration; (B) IPTG-inducible EgTER and DAPG-inducible Pr655 after the promoter swap at varying levels of IPTG concentration; (C) IPTG-inducible TdTER and DAPG-inducible Pr655 at varying levels of IPTG concentrations. All strains harbor cumate-inducible EcAtoB and vanillate-inducible EcFadB in the TriO vector. Cumate and vanillate concentrations are fixed at 5 μM and 10 μM, respectively. IPTG concentration for (A) and DAPG concentrations for (B) and (C) were fixed at 0 μM. Lines are drawn to the mean values with error bars indicating the standard deviation of triplicate biological replicates. (D) Metabolite profiles for FTBOX strains harboring EcAtoB, Pr655, EcFadB, and EgTER or TdTER either all under single inducible promoter (Novagen Duet vector, IPTG-inducible T7 promoter) or under the combination of TriO vector and Novagen Duet vector. Molar concentrations are given on a carbon basis. Bars are drawn to the mean values with error bars indicating the standard deviation of biological triplicates.

address this issue, we explored 1) a more tightly controlled promoter and 2) an alternative thioesterase that is more specific toward butyryl-CoA. For the former, we replaced the T7lac promoter in the pCDFDuet-1 vector with Tet promoter, which is known to have tighter regulation of the lac operon (Lutz and Bujard, 1997). However, basal expression under Tet promoter with no induction was still not successful in decreasing acetate accumulation (Fig. 3).

Alternatively, thioesterase Pr655 from *P. ruminicola* is reported to have high activity toward saturated C4–C5 acids and minimal activity with acetyl-CoA (McMahon and Prather, 2014). When replacing YciA with Pr655 we observed more than 3-fold improvement in rBOX products butyrate and 3-hydroxybutyrate (3HB). However, the best performance was obtained with basal expression (no IPTG addition) and replacement with Tet promoter did not improve performance (Fig. 3). This indicates the need to further balance the expression of core and termination enzymes.

2.5. Addressing enoyl-CoA reductase expression to shift production from 3-hydroxybutyrate to butyrate

Although replacing YciA with Pr655 for the termination appreciably improved the butyrate titer, 3HB was also observed as a major byproduct under tested inducer concentrations in TriO vector (Fig. 3). While the bottleneck from entering the rBOX cycle causes accumulation of either pyruvate or acetate depending on the presence of the termination enzyme, imbalance of rBOX gene expressions often results in accumulation of 3HB, possibly due to thermodynamically favorable NADH-dependent reduction from acetoacetyl-CoA to 3-hydroxybutyryl-CoA (ΔG°_{rxn} = - 13.8 kJ/mol (Flamholz et al., 2012)) and unfavorable dehydration from 3-hydroxybutyryl-CoA to crotonyl-CoA (ΔG°_{rxn} = + 3.3 kJ/mol (Flamholz et al., 2012)), making 3-hydroxybutyryl-CoA a "thermodynamic sink" (Fig. 1). Nevertheless, the subsequent NADH-dependent reduction of crotonyl-CoA to butyryl-CoA is highly exergonic (ΔG°_{rxn} = - 50.6 kJ/mol (Flamholz et al., 2012)), which can drive the flux toward butyryl-CoA production from 3-hydroxybutyryl--CoA with proper balance of expression levels between FadB and EgTER. To validate this hypothesis, we tested increasing EgTER expression by increasing DAPG concentration to direct flux from 3HB to butyrate (Fig. 4A). The impact of DAPG concentration on 3HB and butyrate titers corroborates the hypothesis as higher EgTER expression (higher DAPG concentration) leads to flux shift from 3HB production to butyrate production (Fig. 4A). However, butyrate production appears to saturate at near 10 μM DAPG (1.6 g/L), with 3HB still representing the major rBOX product (2.5 g/L). Interestingly, both butyrate and 3HB production dropped at DAPG concentrations higher than 10 μM. Examination of protein expression in the crude lysates (Fig. S4), revealed that DAPG concentrations of 50 μM and higher cause substantial decrease in Pr655 expression possibly due to the high level of inducer concentration affecting expression from other promoters. The saturation of expression level of DAPG-inducible promoter at near 10 μM DAPG is consistent with the result from the fluorescent protein expression (Fig. 2B). Since T7 is one of the strongest promoters available (Tabor, 1990) and high expression level of thioesterase (Pr655) is not likely needed (see previous section), we performed a promoter swap between EgTER and Pr655, to explore stronger expression of EgTER while also assessing the tightness of the DAPG-inducible promoter (Fig. 4B). As anticipated, EgTER expression driven by the stronger T7 promoter (even at a relatively low IPTG concentration of 10 μM) further shifted the flux from 3HB (1.4 g/L) to butyrate (2.5 g/L) more so than the DAPG induction at the saturating levels (Fig. 4B).

Since 3HB production was still significant, we hypothesized that the kinetic properties of EgTER could be causing a bottleneck in the rBOX pathway and subsequently replaced EgTER with TdTER, which is shown to have superior kinetics with crotonyl-CoA (Hu et al., 2013). Indeed, introduction of TdTER substantially reduced 3HB production across the entire range of IPTG concentrations and completely shifted the flux from 3HB to butyrate (Fig. 4C). Butyrate production was highly dependent on the concentration of IPTG with the highest titer reaching 6.3 g/L at 10 μM IPTG. Under suboptimal inducer concentrations, accumulation of pyruvate was observed instead of acetate or 3HB (Fig. S4b). According to the protein expression analysis, the expression level of TdTER is dominant at 50 μM IPTG and likely affects the expression of other genes due to the limit in the amount of protein expression per cell (Fig. S4a). Of note, when Pr655 was moved to DAPG-inducible promoter, we observed a complete shift in product synthesis from butyrate to acetate with increasing expression (Fig. S4c). This is likely due to promiscuity of the enzyme with acetyl-CoA, consistent with previous observations with YciA. The maximum observed titer for butyrate (6.3 g/L at 10 μM IPTG, 5 μM cumate, 0.1 μM DAPG and 10 μM vanillate addition), represents close to a two-fold increase over previous best titer from the use of a single promoter system without controlled thioesterase expression (Clomburg et al., 2012).

To investigate whether enzyme selection alone was the key driver of improved butyrate production, we constructed the same combination of genes all under T7lac promoter using two Novagen Duet vectors. After testing 5 different IPTG concentrations under the single promoter system, we found accumulation of acetate at IPTG concentrations higher than 5 μM with both EgTER and TdTER (Figs. S4d and S4e). Even with the best result at 1 μM IPTG, only about 1 g/L (with TdTER) and 0.5 g/L (with EgTER) of butyrate was produced with significant 3HB accumulation (Figs. S4d and S4e). In comparison with optimized inducer concentrations using the TriO vector, the butyrate titer when using the single promoter system was only 23% with EgTER and 17% with TdTER (Fig. 4D). Interestingly, under the single promoter system, the product profiles were similar for EgTER or TdTER (Fig. 4D), which indicates that enzyme activities could be misinterpreted under unoptimized relative enzyme concentrations.

2.6. Exploring additional enzyme combinations and inducer concentrations

A key advantage of the TriO vector system is its ability to evaluate the choice of pathway enzymes in a plug-and-play combinatorial manner. To illustrate this, we considered an alternative thiolase (Thl), *Clostridium acetobutylicum* ThlA (CaceThlA) (Stim-Herndon et al., 1995), in place of AtoB, and hydroxyacyl-CoA dehydrogenase (Hacd) and enoyl-CoA hydratase (Ech), *Cupriavidus necator* PhaB1 (Zhang et al., 2019) and *Aeromonas caviae* PhaJ (Fukui et al., 1998), respectively, in place of the bifunctional Hacd-Ech, FadB. These enzymes are known to be viable choices based on literature for catalyzing the corresponding reactions in a one-turn rBOX pathway.

To explore the impact of the Thl choice, we varied the expression of AtoB and CaceThlA (0.1 μM–100 μM cumate) at already identified optimal expression of TdTER (10 μM IPTG), thioesterase Pr655 (0.1 μM DAPG) and FadB (10 μM vanillate). With AtoB, we observed notable butyrate production even at low expression level: between 1 and 3 g/L butyrate at cumate between 0.1 μM and 1 μM (Fig. 5A). The optimum inducer concentration was found to be 10 μM cumate which is identical to that found from the initial run with EgTER and termination via endogenous thioesterases (Fig. S1). Like what was observed from the overexpression of EgTER and TdTER, induction at levels higher than 10 μM caused substantial reduction in butyrate titers (Fig. 5A). When AtoB was replaced with CaceThlA, the trend changed noticeably with almost no butyrate production at low cumate concentrations, and no decrease in product synthesis observed at high cumate levels (Fig. 5B). Analysis of protein expression showed that at low cumate levels, AtoB, which is a native *E. coli* enzyme, could express at sufficient levels to drive carbon flux towards rBOX while expression of heterologous CaceThlA was very low (Fig. S5a). However, at high cumate levels, a significant decrease in AtoB expression was observed at 50 μM and 100 μM cumate, leading to the corresponding drop in butyrate production. In contrast, the expression of CaceThlA stays high even at cumate concentrations up to 100 μM

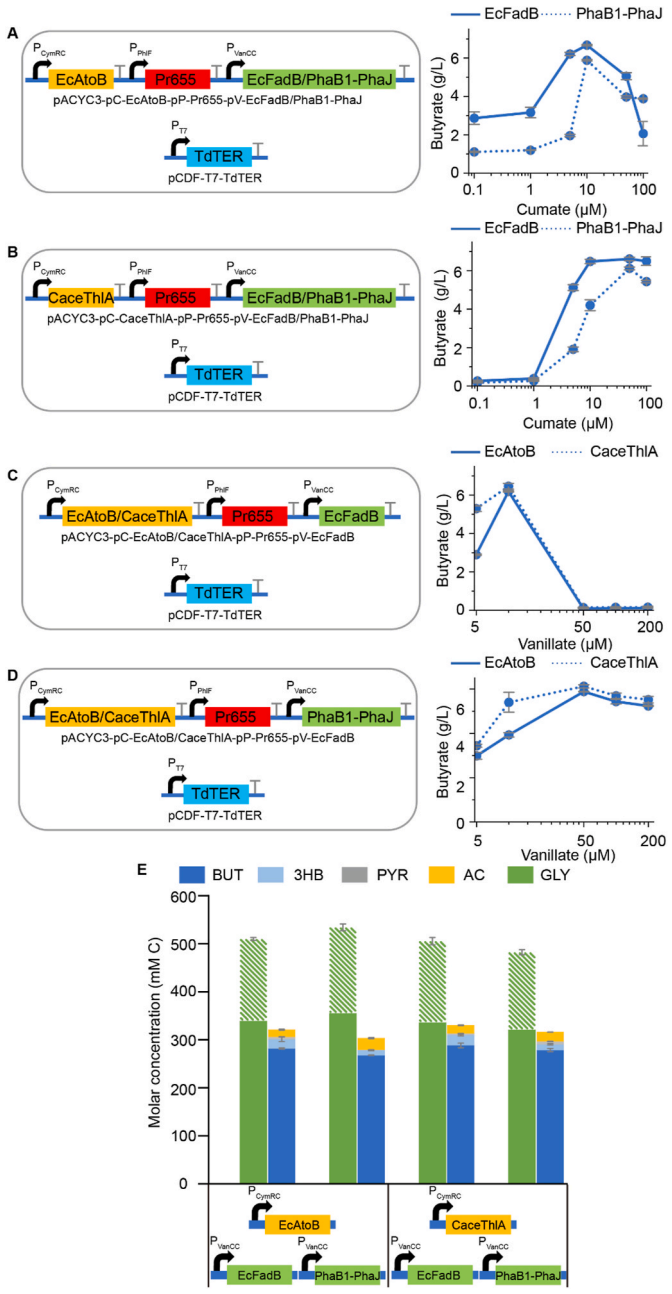

Fig. 5. Enzyme choice and expression level optimization for thiolase and 3-hydroxyacyl-CoA dehydrogenase-enoyl-CoA hydratase (Hacd-Ech) to accomplish global optimum in butyrate production. The effect of cumate concentration on butyrate titer for (A) EcAtoB and (B) CaceThlA, expressed under the cumate-inducible promoter. The effect of vanillate concentration on butyrate titer for (C) EcFadB and (D) PhaB1-PhaJ, expressed under the vanillate-inducible promoter. Symbols represent mean values with error bars indicating the standard deviation of biological triplicates. (E) Glycerol (GLY) consumption and product synthesis at optimal inducer concentrations of four different designs (enzyme combinations) shown in panels (A)–(D). Solid green bars represent theoretical maximum (2/3 of total consumption). Bars are drawn to the mean values with error bars indicating the standard deviation of biological triplicates. In all experiments, TdTER and thioesterase Pr655 were expressed from IPTG- and DAPG-inducible promoters with 10 μM IPTG and 0.1 μM DAPG, respectively.

(Fig. S5a). The trend was similar when PhaB1-PhaJ were employed in place of FadB (under constant 50 μM vanillate) but the solution space for optimum cumate concentrations was narrower demonstrating sharp drop from 10 to 50 μM cumate for AtoB (Fig. 5A), as well as a slight drop in titer was observed at 100 μM cumate with CaceThlA (Fig. 5B).

Next, we assessed the impact of the choice of Hacd and Ech by varying vanillate concentrations while other inducer concentrations were kept constant at previously identified optima. Changes in expression levels of FadB significantly impacted the butyrate production, almost entirely abolishing at vanillate levels of 50 μM or higher with both AtoB and CaceThlA as thiolases (Fig. 5C). Similar to what was seen from AtoB overexpression, protein expression analysis showed that at these high vanillate levels the expression of TdTER and AtoB was substantially reduced, likely due to excessive expression of FadB (Fig. S5b). Interestingly, this was again not the case when heterologous Hacd-Ecd, PhaB1-PhaJ, were employed instead of FadB, as both butyrate production and TdTER and AtoB or CaceThlA (Fig. 5D) expressions stay at high levels, even for high vanillate concentrations (Fig. S5b).

With four different combinations of thiolases and Hacd-Ech tested, we were able to reach maximum butyrate titers between 6.1 g/L and 6.3 g/L at optimum inducer concentrations (Fig. 5A and D). Evaporation during the fermentation did not significantly affect the final volume (Fig. S6) and hence had minimal impact on the final yield (Fig. S7). These titers could be considered "global" optima as they represent close to 90% of the theoretical yield based on the carbon balance: 290 mM carbon of butyrate (6.3 g/L) produced from approximately 500 mM carbon of glycerol consumed (333 mM being the theoretical maximum yield) (Fig. 5E). The observed trends for product concentrations mirror similar trends in production rates/fluxes, as can be seen from the time-course analysis of growth and product synthesis in these strains (Fig. S8). Both product titers (6.1–6.3 g/L) and specific rates/fluxes (0.09–0.14 g/gDCW/h) were remarkably similar for all four strains.

2.7. *Expanding the pathways for a different termination route and higher-order iterations*

Having established the TriO vector system for butyrate synthesis, we explored a different termination route by reduction of butyryl-CoA to butyraldehyde and then to n-butanol, catalyzed by acyl-CoA reductase (Acr) and alcohol dehydrogenase (Adh), respectively (Fig. 6A and B). We previously reported that acyl-CoA reductase from *Clostridium beijerinkii* (CbAld) has high activity toward butyryl-CoA reduction (Kim et al., 2015). CbAld combined with *E. coli* alcohol dehydrogenase (FucO) were incorporated under DAPG-inducible promoter slot replacing Pr655 while other genes (AtoB/CaceThlA, TdTER and FadB/PhaB1-PhaJ) remained under the same promoters. Unlike the case of thioesterase (Pr655), where 0.1 μM DAPG addition was sufficient to drive the flux toward butyryl-CoA hydrolysis, CbAld-FucO termination required DAPG concentration of 5 μM and higher to drive the flux toward n-butanol synthesis (Fig. 6C). At concentrations above this level, a saturation in expression was observed as indicated by plateau in n-butanol titer, which is consistent with fluorescent protein analysis (Fig. 2B). At low DAPG concentrations below 5 μM, an accumulation of pyruvate was observed with no rBOX product, indicating no flux entering the rBOX pathways due to the absence of outlet (termination enzymes) (Fig. S10). The trend in n-butanol production with changing expression levels of AtoB, FadB and TdTER (Fig. 6C) was very similar to what was observed with butyrate production indicating optimal relative expression levels of core rBOX enzymes are not significantly affected by the change in termination enzymes. However, testing different enzyme combinations revealed that PhaB1-PhaJ resulted in significant decrease in n-butanol titer compared to FadB, which was the key difference from butyrate production (Fig. 6D). On the other hand, replacing thiolase from AtoB to CaceThlA did not result in notable change in n-butanol titer although slightly higher pyruvate accumulation was observed (Fig. 6D and Fig. S9f). Overall, we observed n-butanol titer reaching 2.2 g/L upon

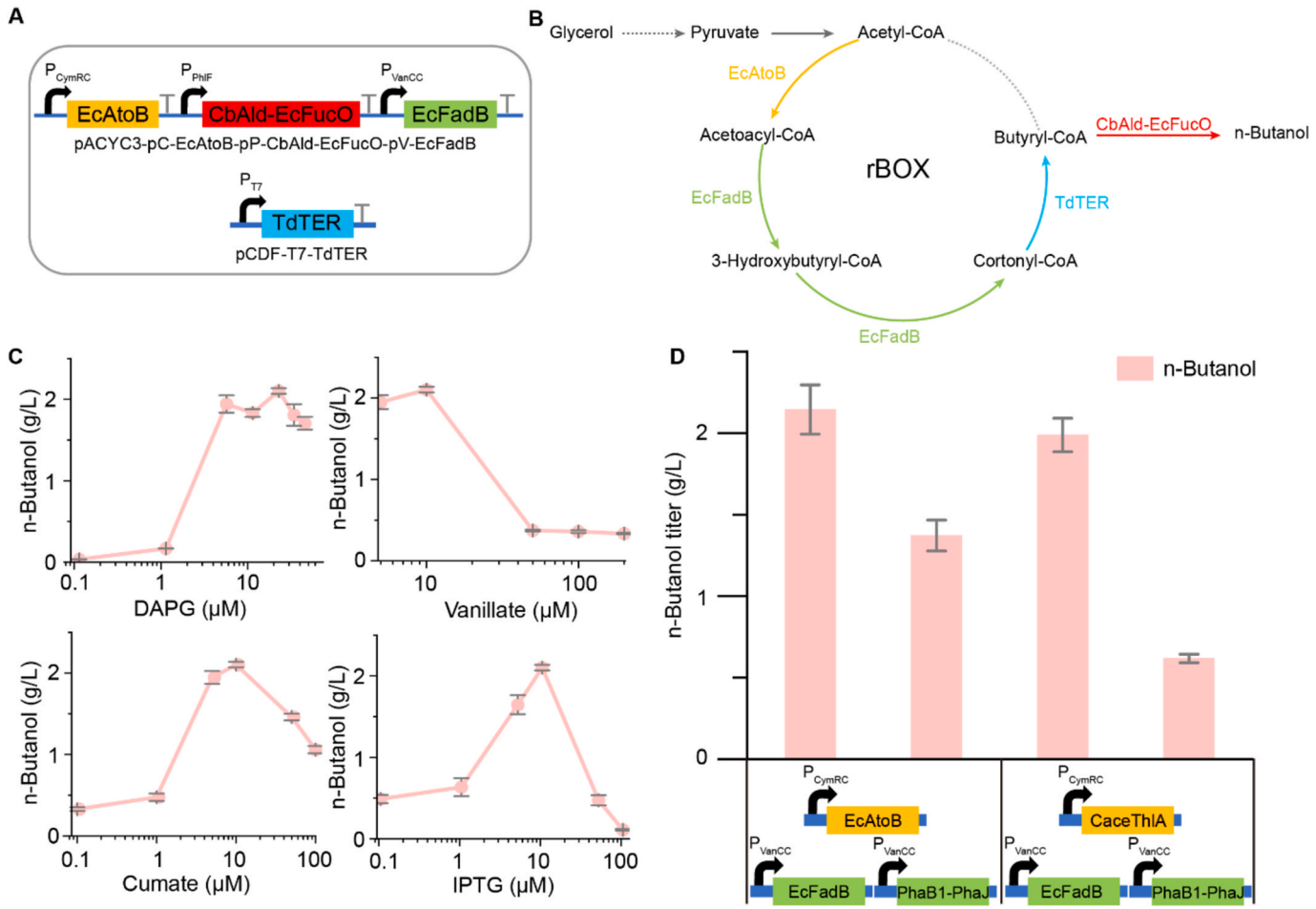

Fig. 6. N-Butanol production from one-turn rBOX by employing acyl-CoA reductase (CbAld) and alcohol dehydrogenase (EcFucO) as termination enzymes. (A) Plasmids used for n-butanol production. (B) Simplified schematic for the production of n-Butanol from glycerol. (C) The effect of inducer concentrations on n-butanol titer for CbAld-EcFucO expressed under the DAPG-inducible promoter; EcFadB expressed under vanillate-inducible promoter; EcAtoB expressed under cumate-inducible promoter; and TdTER expressed under IPTG-inducible T7 promoter. Symbols represent mean values with error bars indicating the standard deviation of biological triplicates. (D) n-Butanol titer from four different enzyme combinations tested for butyrate production under the same optimal inducer concentrations for butyrate production. DAPG concentration was constant at 20 μM. Bars are drawn to the mean values with error bars indicating the standard deviation of biological triplicates.

optimization of relative inducer concentrations.

Next, we explored the rBOX pathways with two full iterations for hexanoate synthesis using TriO vector system. While the core elongation enzymes FadB for Hacd-Ech and TdTER for Ter are known to have a broad substrate specificity including C4 and C6 substrates, both thiolases (AtoB and CaceThlA) and thioesterase (Pr655) are reported to have a high specificity toward C4 (McMahon and Prather, 2014; Vögeli et al., 2022). Alternatively, thiolase from *Clostridium kluyveri* (CkThlA) (Vögeli et al., 2022) and an engineered variant of *E. coli* thioesterase 'TesA M141L E142D Y145G (Deng et al., 2020) (TesA* from here on) are reported to have high specificity toward medium-chain acyl-CoAs including C6. Therefore, CkThlA and TesA* were introduced replacing AtoB/CaceThlA and Pr655 under cumate-inducible and DAPG-inducible promoters from the butyrate producing strain, respectively (Fig. 7A and B). In addition to investigating the relative expression of the two newly introduced genes, we explored all four gene expressions in parallel because optimal relative expression levels could be different from single iteration reactions. While the TdTER expression in relation to the hexanoate titer showed similar profile as butyrate having a sharp peak at 10 μM IPTG, FadB expression exhibited a shift in optimum from 10 μM in butyrate production to 5 μM (Fig. 7C). Another interesting observation was the absence of other byproducts than pyruvate (Fig. S10), which is strikingly different from butyrate example which showed significant accumulation of 3HB and acetate under unbalanced expression levels of pathway genes. This could be because the termination enzyme TesA* (Clomburg et al., 2012; Deng et al., 2020) is highly specific toward saturated medium-chain acyl-CoAs as opposed to YciA (Clomburg et al., 2012) or Pr655 (McMahon and Prather, 2014) which have promiscuous activities with acetyl-CoA and 3-hydroxybutyryl-CoA. Similar behavior was observed during n-butanol production with CbAld, which is highly specific toward butyryl-CoA reduction.

Upon optimization of all four inducer concentrations, we obtained hexanoate titer of 4.0 g/L with carbon yield reaching near 70% of the theoretical yield. Unlike the case of butyrate production, we still observed significant production of pyruvate (~25% from all products), which indicates room for further optimization.

3. Discussion

In this study, we employed a plasmid-based orthogonal inducible promoter system (TriO vectors) for meticulous control of relative expression levels in rBOX pathway enzymes. Varying relative expression levels demonstrated dramatic impact on metabolic flux and product profile from no production to up to 90% theoretical yield of the target products. Using different termination enzymes and multiple iterations, we explored different rBOX products, including butyrate, n-butanol and

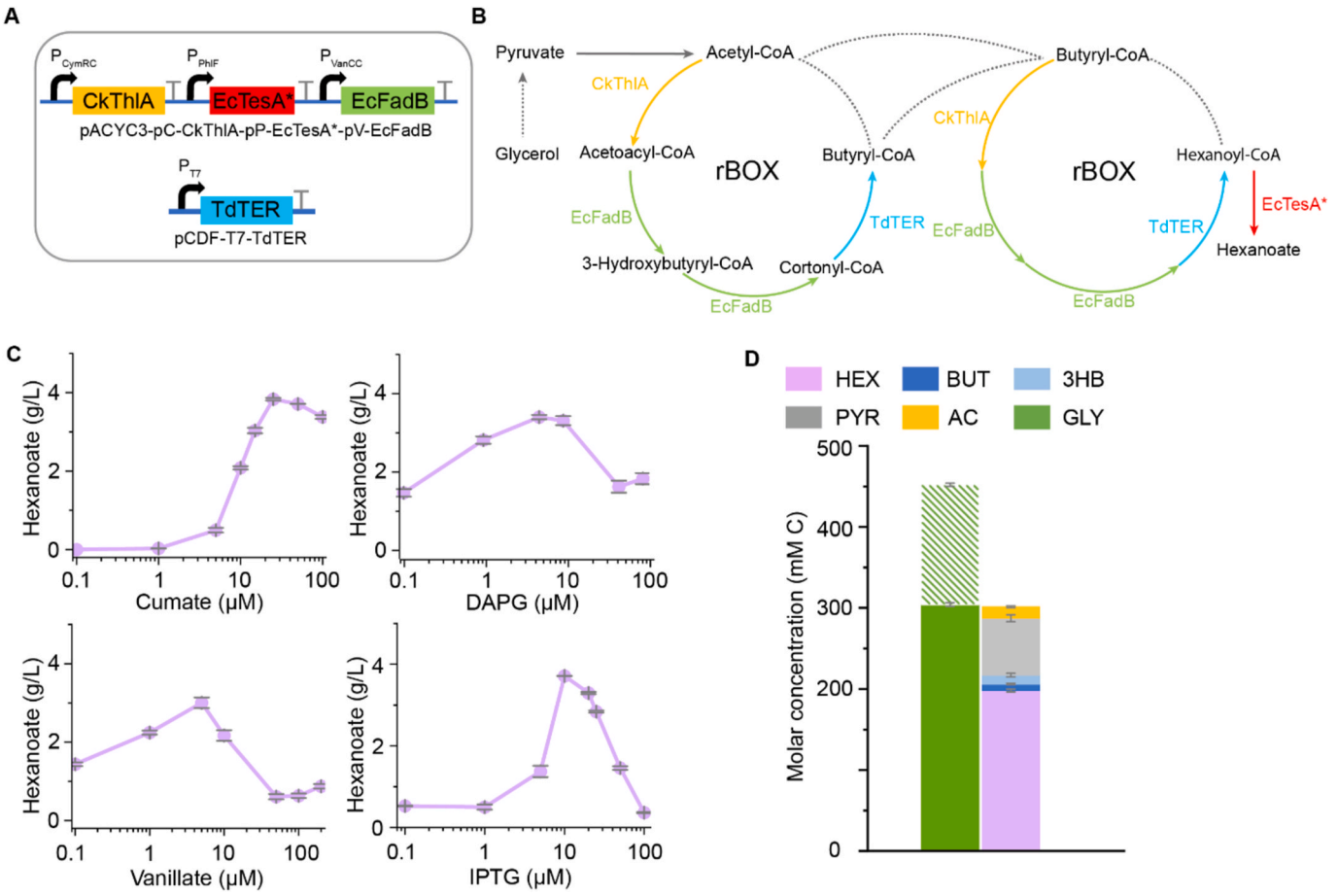

Fig. 7. Hexanoate production from two-turn rBOX by using alternative priming (thiolase) and termination (thioesterase) enzymes. (A) Plasmids used for hexanoate production. (B) Simplified schematic for the production of hexanoate from glycerol. (C) The effect of inducer concentrations on hexanoate titer on CkThlA expressed under the cumate-inducible promoter; EcTesA* expressed under the DAPG-inducible promoter; EcFadB expressed under the vanillate-inducible promoter; and TdTER expressed under the T7lac promoter. Symbols represent mean values with error bars indicating the standard deviation of biological triplicates. (D) Glycerol consumption and product profile at optimal inducer concentrations for hexanoate (HEX) production. Solid green bar represents theoretical maximum. Bars are drawn to the mean values with error bars indicating the standard deviation of biological triplicates.

hexanoate. In all cases, the impact of changing relative expression levels was prominent with similar observations. Upon optimization of the pathway enzyme concentrations, we obtained the titer of 6.3 g/L butyrate, 2.2 g/L butanol and 4.0 g/L hexanoate from glycerol in *E. coli*, exceeding the best titers from the previous reports using identical enzyme combinations (Clomburg et al., 2012; Vögeli et al., 2022).

Exploring various expression levels of individual genes uncovered interesting findings from the rBOX pathway, previously unnoticed due to the inability to explore the entire solution space of relative expression levels. For example, it is remarkable that four different combinations of pathway enzymes employed for butyrate production all resulted in the same "global optimum" of approximately 6.3 g/L titer. With the butyrate yield reaching 90% of the theoretical maximum yield, there is minimal room for further improvement under the tested condition indicating near complete debottlenecking of the pathway flux. In each design, there were notable differences in the product profile with changing individual gene expression levels. For example, it appears significantly higher induction levels of heterologous CaceThlA is required to achieve comparative flux with native AtoB, but AtoB exhibits narrower range of optimal expression levels (Fig. 5A and B). Similar behavior was observed in comparison native FadB and heterologous PhaB1-PhaJ for Hacd-Ech. We could hypothesize that native *E. coli* genes, *atoB* and *fadB* have better inherent expression levels, which in turn lead to higher efficiency as less resources would be required to achieve the same performance. Given that protein expression is one of the most energy-intensive cellular activities (Marquez-Zavala and Utrilla, 2023), identifying enzymes with high efficiency could be the key consideration for introducing pathways with less burden. On the other hand, from the perspective of the stability and robustness of the system, one could argue that a wide range of saturation region as opposed to sharp optimum provides a better stability of the system, which would favor CaceThlA and PhaB1-PhaJ over AtoB and FadB. The stability of the system could be the reason for observing better performance of CaceThlA compared to AtoB in a separate report (Yang et al., 2019), in which balancing relative expression levels was not investigated. The tradeoff between efficiency and stability observed from this example is likely a common feature in many other designs and the TriO system provides a tool to investigate and find a suitable solution in a rapid, cost-efficient manner. We conducted a preliminary study on the production rates and found that under optimal inducer concentrations both volumetric as well as specific rates (i.e. fluxes) corresponding to different enzyme combinations are very similar (Fig. S8).

Exploring a different termination route for n-butanol production or multiple iterations for hexanoate production also allowed debottlenecking of the pathway, albeit not at the levels of butyrate, as indicated from achieved titer and carbon yields (Figs. 6 and 7). In the case of n-butanol production, the requirement of two additional NADH for butyryl-CoA reduction could influence the upstream pathway flux leading to different flux profiles. These factors might have caused the substantial difference between FadB and PhaB1-PhaJ as Hacd-Ech for n-

butanol production (Fig. 6E). However, the general trends in relationship between core enzyme expression between butyrate and n-butanol were identical, indicating the impact of relative expression of core rBOX enzymes on the one-turn iteration remains largely unchanged despite the difference in termination pathways. On the other hand, multiple iterations that involve repeated catalysis of core enzymes on different chain length intermediates (C4 and C6) likely caused notable shift in optimal expression levels toward higher induction for common enzymes like FadB and TdTER (Fig. 7C and D). This phenomenon is consistent with a recent study on *in vitro* analysis of the impact of relative enzyme concentrations in product chain-lengths in rBOX pathway, where higher concentration of core pathway enzymes (thiolase and Hacd-Ech) led to increased ratio of longer chain products (Courtney et al., 2023), albeit a mixture of rBOX products was still observed. The requirement of high thiolase expression could have caused the saturation in CkThlA expression levels at cumate higher than 20 μM (Fig. 7A), a saturation level in Cym promoter consistent with the fluorescent protein analysis (Fig. 2). This could be an indication of suboptimal kinetics of this enzyme, where a proper assessment of kinetic parameters and modeling could elucidate an appropriate solution for further improving the product titer and specificity.

A key advantage of the orthogonal inducible promoter system employed in this study is its ability to directly monitor the relationship between individual pathway gene expression and product profiles that provides understanding of the metabolic flux distribution. While the objective of optimizing relative gene expression can also be achieved by employing libraries of promoter and/or RBS for each gene, the cost for DNA synthesis and infrastructure for high throughput screening of multi-enzyme pathways like rBOX is often beyond the budget of an academic laboratory (Park et al., 2023). Combining the Marionette orthogonal inducible promoter system (Meyer et al., 2019) with a Golden Gate based modular cloning method maximizes the amount of accessible enzyme solution space that can be explored with a minimal amount of DNA and strain construction. In a sense, our system is democratizing the testing and evaluation of pathway designs at low cost and significantly reduced time and infrastructure commitment.

We believe the TriO vector system or similar tools can substantially expand our understanding and capabilities of many other metabolic pathways beyond rBOX pathways as seen from recent examples (Meyer et al., 2019; Park et al., 2023). However, more study needs to be done in how the optimal relative expression level translates during scale up or with the use of different carbon sources or media. Given the inducible nature of TriO, we can envision introduction of dynamic regulatory systems to decouple production from cell growth, allowing better scalability and transferability to various fermentation systems and conditions (Ni et al., 2021; Ye et al., 2021). In terms of industrial applications where expensive antibiotics and inducer molecules are not suitable, the relative strengths of gene expression identified from rational optimization of inducer concentrations could be transferred into genome-integrated constitutive promoter systems by adjusting the promoter and RBS strengths accordingly (Hossain et al., 2020; LaFleur et al., 2022). This way, the substantial amount of time and cost associated with extensive library construction and screening can be avoided. Alternatively, various inexpensive biosensors can be combined with orthogonal gene regulation systems to accomplish the same objective without the need for costly small inducer molecules (Koch et al., 2019). Overall, the TriO vector system and similar tools that allow orthogonal control of relative gene expressions has a great potential in advancing the field of metabolic engineering and biomanufacturing.

4. Methods

4.1. Reagents

All chemicals were obtained from Fisher Scientific Co. and Sigma-Aldrich Co. unless otherwise specified. Primers were synthesized by Integrated DNA Technologies or by Azenta Life Sciences. Restriction enzymes were obtained from New England Biolabs unless otherwise specified.

5. Plasmids, strains and genetic methods

Plasmid-based gene expression was achieved by cloning the desired gene(s) into pETDuet-1, pCDFDuet-1 (Novagen), pCEntry, pPEntry, and pVEntry digested with appropriate restriction enzymes and by using In-Fusion cloning technology (Clontech Laboratories, Inc.). Linear DNA fragments for insertion were created via PCR of the open reading frame of interest from the genomic DNA (for genes native to *E. coli*) or from plasmids used in our previous works (Cheong et al., 2016; Kim et al., 2015; Vögeli et al., 2022). Pr655 was synthesized by Twist Biosciences as DNA fragments and integrated into the Entry vectors via In-Fusion assembly. In-Fusion assembly products were used to transform *E. coli* Stellar cells (Clontech Laboratories, Inc.), and clones identified by PCR screening were further confirmed by DNA sequencing. The completed pCEntry, pPEntry and pVEntry vectors were assembled with pACYC3 Destination vector via Golden Gate Assembly using Golden Gate Assembly Kit (*Bsa*I-HF v2, New England Biolabs). Plasmids used in this study are listed in Supplementary Table 1. The Marionette Sensor Collection was a gift from Christopher Voigt (Addgene Kit #1000000137).

JST07 (DE3) (Kim et al., 2015) (Wild-type K12 *Escherichia coli* strain MG1655 λDE3 *ΔldhA*::FRT *ΔpoxB*::FRT *Δpta*::FRT *ΔadhE*::FRT *ΔfrdA*::FRT *ΔyciA*::FRT *ΔybgC*::FRT *ΔydiI*::FRT *ΔtesA*::FRT *ΔfadM*::FRT *ΔtesB*::FRT *ΔfadE*::FRT) was used as the host for all genetic modifications. Genomic modifications were created using a CRISPR-Cas9-based system developed for *E. coli* (Jiang et al., 2015). pCas and pTargetF were gifts from S. Yang (Addgene plasmids nos. 62,225 and 62,226, respectively). Strains used in this study are listed in Supplementary Table S1.

5.1. Fluorescent protein assay using TriO vector

FTBOX strain harboring pACYC3-pC-eYFP-pP-mRFP-pV-eGFP and pCDFDuet-1-P1-eBFP2 was inoculated (1%) into 30 mL of LB media containing the appropriate antibiotics from an overnight LB culture. 250 μL of the inoculated media was then distributed into the wells of a 2 mL deep, square 96-well plate. Plates containing inoculated media were covered with a rayon microporous film (USA Scientific) and incubated in an incubating microplate shaker (VWR International) at 30 °C and 1000 rpm. After 2.5 h, 1 μL of inducers were added from stock solutions to achieve the indicated final concentrations. 24 h after inoculation, cells were pelleted by centrifugation (3220×*g*, 8 min) and the pellet resuspended with 1 mL of M9 basal salt media without carbon source. 100 μL of the cell suspension was transferred to a 96-well black, clear bottom plate. A Synergy H1 microplate reader (Biotek) was used to measure the OD600 and fluorescence at the following excitation and emissions: eYFP (515, 541), mRFP1 (584, 621), eGFP (460, 500), eBFP2 (382, 448).

5.2. Culture medium and cultivation conditions

The minimal medium designed by Neidhardt et al. (1974), with 125 mM MOPS and Na_2HPO_4 in place of K_2HPO_4, supplemented with 20 g/L glycerol, 10 g/L tryptone, 5 g/L yeast extract, 100 μM FeSO4, 1.48 mM Na_2HPO_4, 5 mM $(NH_4)_2SO_4$, and 30 mM NH_4Cl was used for all fermentations unless otherwise stated. Antibiotics (100 μg/mL carbenicillin, 100 μg/mL spectinomycin and 34 μg/mL chloramphenicol) and appropriate levels of inducers (isopropyl β-D-1-thiogalactopyranoside (IPTG), cumate, 2,4-diacetylphophloroglucinol and vanillate) were added.

Fermentations were conducted in 25 mL Pyrex Erlenmeyer fasks (narrow mouth/heavy duty rim, Corning Inc., Corning, NY) filled with 10 mL (for butanol production, 20 mL were used instead of 10 mL) of the above culture medium and sealed with foam plugs filling the necks. A

single colony of the desired strain was cultivated overnight (14–16 h) in LB medium with appropriate antibiotics and used as the inoculum (1%) for all fermentations. After inoculation, flasks were incubated at 37 °C and 200 rpm in an NBS C24 Benchtop Incubator Shaker (New Brunswick Scientific Co., Inc., Edison, NJ) until an optical density of ~0.3–0.5 was reached, at which point IPTG, cumate, DAPG and vanillate were added. Flasks were then incubated under the same conditions for 48 h post-induction unless otherwise stated.

5.3. Analytical methods

Optical density was measured at 600 nm in a Thermo Spectronic 200 (Thermo Scientific, Waltham, MA) and used as an estimate of cell mass (1 OD_{600} nm = 0.34 g dry cell weight/L). pH was measured using pH meter (Sartorius, Göttingen, Germany). Fermentation products are harvested, and the supernatant was analyzed by high-performance liquid chromatography (HPLC) using a Prominence SIL-20 system (Shimadzu Scientific Instruments) equipped with a refractive index detector and an HPX-87H organic acid column (Bio-Rad) with operating conditions to optimize peak separation (0.3 mL/min flow rate, 30 mM H_2SO_4 mobile phase, column temperature of 42 °C). Data were acquired and analyzed using Shimadzu LabSolutions v5.96. Volumetric rates were calculated based on the change in titer over time, using formula Q = (C2 – C1)/(t2 - t1); specific rates (i.e. product fluxes) were determined by dividing the change in titer over time by the cell mass, following the formula q = (C2 – C1)/(t2 - t1)/Average cell mass, where 'C' represents concentration and 't' represents time. Cell pellets harvested were resuspended to ~40 OD_{600} in B-PER® Bacterial Protein Extraction Reagent (Thermo Fisher) supplemented with 0.1 mg/mL chicken egg white lysozyme and 5 U/mL Benzonase® nuclease for cell lysis. After incubation in room temperature for 15 min, 100 μL of each cell lysate was transferred to 1.5 mL microcentrifuge tubes for centrifugation at 15,000×*g* for 5 min. The soluble cell lysates obtained from the supernatant were analyzed using SDS-PAGE (10% PAGE gel) following the manufacturer instructions.

Competing financial interests statement

R.G. is the sole proprietor of RBN Biotech LLC, which holds rights to several r-BOX patents. All other authors declare no competing interests.

CRediT authorship contribution statement

Seung Hwan Lee: Formal analysis, Investigation, Methodology, Writing – original draft, Writing – review & editing, Conceptualization. **Yang Hu:** Investigation, Methodology, Writing – original draft, Writing – review & editing, Formal analysis. **Alexander Chou:** Investigation, Methodology, Writing – original draft, Writing – review & editing. **Jing Chen:** Investigation, Methodology, Writing – original draft, Writing – review & editing. **Ramon Gonzalez:** Conceptualization, Funding acquisition, Project administration, Supervision, Writing – original draft, Writing – review & editing.

Data availability

All data supporting the findings of this study are included in the paper and its supplementary information. The following plasmids can be acquired from Addgene: pCEntry (Plasmid #207672); pPEntry (Plasmid #207673); pVEntry (Plasmid #207674); pACYC Destination (Plasmid #207675).

Acknowledgements

This work was funded by the US Department of Energy (award numbers DE-EE0008499 and DE-EE0008343) and the US National Science Foundation (award number CBET-1805793).

Appendix A. Supplementary data

Supplementary data to this article can be found online at https://doi.org/10.1016/j.ymben.2024.02.007.

References

Cheong, S., Clomburg, J.M., Gonzalez, R., 2016. Energy- and carbon-efficient synthesis of functionalized small molecules in bacteria using non-decarboxylative Claisen condensation reactions. Nat. Biotechnol. 34 (5), 556–561. https://doi.org/10.1038/nbt.3505.

Clomburg, J.M., Blankschien, M.D., Vick, J.E., Chou, A., Kim, S., Gonzalez, R., 2015. Integrated engineering of beta-oxidation reversal and omega-oxidation pathways for the synthesis of medium chain omega-functionalized carboxylic acids. Metab. Eng. 28, 202–212. https://doi.org/10.1016/j.ymben.2015.01.007.

Clomburg, J.M., Vick, J.E., Blankschien, M.D., Rodriguez-Moya, M., Gonzalez, R., 2012. A synthetic biology approach to engineer a functional reversal of the beta-oxidation cycle. ACS Synth. Biol. 1 (11), 541–554. https://doi.org/10.1021/sb3000782.

Courtney, D.K., Su, Y., Jacobson, T.B., Khana, D.B., Ailiani, A., Amador-Noguez, D., Pfleger, B.F., 2023. Relative activities of the β-ketoacyl-CoA and acyl-CoA reductases influence the product profile and flux in a reversed β-oxidation pathway. ACS Catal. 5914–5925. https://doi.org/10.1021/acscatal.3c00379.

Dellomonaco, C., Clomburg, J.M., Miller, E.N., Gonzalez, R., 2011. Engineered reversal of the beta-oxidation cycle for the synthesis of fuels and chemicals. Nature 476 (7360), 355–359. https://doi.org/10.1038/nature10333.

Deng, X., Chen, L., Hei, M., Liu, T., Feng, Y., Yang, G.Y., 2020. Structure-guided reshaping of the acyl binding pocket of 'TesA thioesterase enhances octanoic acid production in E. coli. Metab. Eng. 61, 24–32. https://doi.org/10.1016/j.ymben.2020.04.010.

Flamholz, A., Noor, E., Bar-Even, A., Milo, R., 2012. eQuilibrator–the biochemical thermodynamics calculator. Nucleic Acids Res. 40 (Database issue), D770–D775. https://doi.org/10.1093/nar/gkr874.

Fleur, T.L., Hossain, A., Salis, H.M., 2021. Automated model-predictive design of synthetic promoters to control transcriptional profiles in bacteria. bioRxiv. https://doi.org/10.1101/2021.09.01.458561, 2021.2009.2001.458561.

Fukui, T., Shiomi, N., Doi, Y., 1998. Expression and characterization of (R)-specific enoyl coenzyme A hydratase involved in polyhydroxyalkanoate biosynthesis by Aeromonas caviae. J. Bacteriol. 180 (3), 667–673. https://doi.org/10.1128/JB.180.3.667-673.1998.

Harder, B.J., Bettenbrock, K., Klamt, S., 2018. Temperature-dependent dynamic control of the TCA cycle increases volumetric productivity of itaconic acid production by Escherichia coli. Biotechnol. Bioeng. 115 (1), 156–164. https://doi.org/10.1002/bit.26446.

Hossain, A., Lopez, E., Halper, S.M., Cetnar, D.P., Reis, A.C., Strickland, D., Klavins, E., Salis, H.M., 2020. Automated design of thousands of nonrepetitive parts for engineering stable genetic systems. Nat. Biotechnol. 38 (12), 1466–1475. https://doi.org/10.1038/s41587-020-0584-2.

Hu, K., Zhao, M., Zhang, T., Zha, M., Zhong, C., Jiang, Y., Ding, J., 2013. Structures of trans-2-enoyl-CoA reductases from Clostridium acetobutylicum and Treponema denticola: insights into the substrate specificity and the catalytic mechanism. Biochem. J. 449 (1), 79–89. https://doi.org/10.1042/BJ20120871.

Jiang, Y., Chen, B., Duan, C., Sun, B., Yang, J., Yang, S., 2015. Multigene editing in the Escherichia coli genome via the CRISPR-Cas9 system. Appl. Environ. Microbiol. 81 (7), 2506–2514. https://doi.org/10.1128/AEM.04023-14.

Kim, S., Clomburg, J.M., Gonzalez, R., 2015. Synthesis of medium-chain length (C6-C10) fuels and chemicals via beta-oxidation reversal in Escherichia coli. J. Ind. Microbiol. Biotechnol. 42 (3), 465–475. https://doi.org/10.1007/s10295-015-1589-6.

Kim, S., Gonzalez, R., 2018. Selective production of decanoic acid from iterative reversal of beta-oxidation pathway. Biotechnol. Bioeng. 115 (5), 1311–1320. https://doi.org/10.1002/bit.26540.

Koch, M., Pandi, A., Borkowski, O., Batista, A.C., Faulon, J.L., 2019. Custom-made transcriptional biosensors for metabolic engineering. Curr. Opin. Biotechnol. 59, 78–84. https://doi.org/10.1016/j.copbio.2019.02.016.

Kroll, J., Klinter, S., Schneider, C., Voss, I., Steinbuchel, A., 2010. Plasmid addiction systems: perspectives and applications in biotechnology. Microb. Biotechnol. 3 (6), 634–657. https://doi.org/10.1111/j.1751-7915.2010.00170.x.

LaFleur, T.L., Hossain, A., Salis, H.M., 2022. Automated model-predictive design of synthetic promoters to control transcriptional profiles in bacteria. Nat. Commun. 13 (1), 5159. https://doi.org/10.1038/s41467-022-32829-5.

Laguna, R., Young, S.J., Chen, C.C., Ruiz, N., Yang, S.T., Tabita, F.R., 2015. Development of a plasmid addicted system that is independent of co-inducers, antibiotics and specific carbon source additions for bioproduct (1-butanol) synthesis in Escherichia coli. Metab Eng Commun 2, 6–12. https://doi.org/10.1016/j.meteno.2014.12.001.

Lee, M.E., Aswani, A., Han, A.S., Tomlin, C.J., Dueber, J.E., 2013. Expression-level optimization of a multi-enzyme pathway in the absence of a high-throughput assay. Nucleic Acids Res. 41 (22), 10668–10678. https://doi.org/10.1093/nar/gkt809.

Lee, S.H., Chou, A., Nattermann, M., Zhu, F., Clomburg, J.M., Paczia, N., Erb, T.J., Gonzalez, R., 2023. Identification of 2-hydroxyacyl-CoA synthases with high acyloin condensation activity for orthogonal one-carbon bioconversion. ACS Catal. 12007–12020. https://doi.org/10.1021/acscatal.3c02373.

Lutz, R., Bujard, H., 1997. Independent and tight regulation of transcriptional units in Escherichia coli via the LacR/O, the TetR/O and AraC/I1-I2 regulatory elements. Nucleic Acids Res. 25 (6), 1203–1210. https://doi.org/10.1093/nar/25.6.1203.

Marquez-Zavala, E., Utrilla, J., 2023. Engineering resource allocation in artificially minimized cells: is genome reduction the best strategy? Microb. Biotechnol. https://doi.org/10.1111/1751-7915.14233.

McMahon, M.D., Prather, K.L., 2014. Functional screening and in vitro analysis reveal thioesterases with enhanced substrate specificity profiles that improve short-chain fatty acid production in Escherichia coli. Appl. Environ. Microbiol. 80 (3), 1042–1050. https://doi.org/10.1128/AEM.03303-13.

Meyer, A.J., Segall-Shapiro, T.H., Glassey, E., Zhang, J., Voigt, C.A., 2019. Escherichia coli "Marionette" strains with 12 highly optimized small-molecule sensors. Nat. Chem. Biol. 15 (2), 196–204. https://doi.org/10.1038/s41589-018-0168-3.

Neidhardt, F.C., Bloch, P.L., Smith, D.F., 1974. Culture medium for enterobacteria. J. Bacteriol. 119 (3), 736–747. https://doi.org/10.1128/jb.119.3.736-747.1974.

Ni, C., Dinh, C.V., Prather, K.L.J., 2021. Dynamic control of metabolism. Annu. Rev. Chem. Biomol. Eng. 12, 519–541. https://doi.org/10.1146/annurev-chembioeng-091720-125738.

Park, J.H., Bassalo, M.C., Lin, G.M., Chen, Y., Doosthosseini, H., Schmitz, J., Roubos, J. A., Voigt, C.A., 2023. Design of four small-molecule-inducible systems in the yeast chromosome, applied to optimize terpene biosynthesis. ACS Synth. Biol. https://doi.org/10.1021/acssynbio.2c00607.

Peccoud, J., Weber, E., Engler, C., Gruetzner, R., Werner, S., Marillonnet, S., 2011. A modular cloning system for standardized assembly of multigene constructs. PLoS One 6 (2). https://doi.org/10.1371/journal.pone.0016765.

Reis, A.C., Salis, H.M., 2020. An automated model test system for systematic development and improvement of gene expression models. ACS Synth. Biol. 9 (11), 3145–3156. https://doi.org/10.1021/acssynbio.0c00394.

Stephanopoulos, G., Aristidou, A.A., Nielsen, J., 1998. Metabolic Engineering: Principles and Methodologies. Elsevier Science. https://books.google.com/books?id=9mGzkso4NVQC.

Stim-Herndon, K.P., Petersen, D.J., Bennett, G.N., 1995. Characterization of an acetyl-CoA C-acetyltransferase (thiolase) gene from Clostridium acetobutylicum ATCC 824. Gene 154 (1), 81–85. https://doi.org/10.1016/0378-1119(94)00838-J.

Tabor, S., 1990. Expression using the T7<scp>RNA</scp>Polymerase/Promoter system. Curr. Protoc. Mol. Biol. 11 (1) https://doi.org/10.1002/0471142727.mb1602s11.

Tan, Z., Clomburg, J.M., Cheong, S., Qian, S., Gonzalez, R., 2020. A polyketoacyl-CoA thiolase-dependent pathway for the synthesis of polyketide backbones. Nat. Catal. 3 (7), 593–603. https://doi.org/10.1038/s41929-020-0471-8.

Tarasava, K., Lee, S.H., Chen, J., Kopke, M., Jewett, M.C., Gonzalez, R., 2022. Reverse beta-oxidation pathways for efficient chemical production. J. Ind. Microbiol. Biotechnol. https://doi.org/10.1093/jimb/kuac003.

Vögeli, B., Schulz, L., Garg, S., Tarasava, K., Clomburg, J.M., Lee, S.H., Gonnot, A., Moully, E.H., Kimmel, B.R., Tran, L., Zeleznik, H., Brown, S.D., Simpson, S.D., Mrksich, M., Karim, A.S., Gonzalez, R., Kopke, M., Jewett, M.C., 2022. Cell-free prototyping enables implementation of optimized reverse beta-oxidation pathways in heterotrophic and autotrophic bacteria. Nat. Commun. 13 (1), 3058. https://doi.org/10.1038/s41467-022-30571-6.

Yang, H., Huang, B., Lai, N., Gu, Y., Li, Z., Ye, Q., Wu, H., 2019. Metabolic engineering of Escherichia coli carrying the hybrid acetone-biosynthesis pathway for efficient acetone biosynthesis from acetate. Microb. Cell Factories 18 (1), 6. https://doi.org/10.1186/s12934-019-1054-8.

Ye, Z., Li, S., Hennigan, J.N., Lebeau, J., Moreb, E.A., Wolf, J., Lynch, M.D., 2021. Two-stage dynamic deregulation of metabolism improves process robustness & scalability in engineered E. coli. Metab. Eng. 68, 106–118. https://doi.org/10.1016/j.ymben.2021.09.009.

Yin, X., Shin, H.D., Li, J., Du, G., Liu, L., Chen, J., 2017. Pgas, a low-pH-induced promoter, as a tool for dynamic control of gene expression for metabolic engineering of Aspergillus Niger. Appl. Environ. Microbiol. 83 (6) https://doi.org/10.1128/AEM.03222-16.

Zhang, M., Kurita, S., Orita, I., Nakamura, S., Fukui, T., 2019. Modification of acetoacetyl-CoA reduction step in Ralstonia eutropha for biosynthesis of poly(3-hydroxybutyrate-co-3-hydroxyhexanoate) from structurally unrelated compounds. Microb. Cell Factories 18 (1), 147. https://doi.org/10.1186/s12934-019-1197-7.

Zhao, E.M., Zhang, Y., Mehl, J., Park, H., Lalwani, M.A., Toettcher, J.E., Avalos, J.L., 2018. Optogenetic regulation of engineered cellular metabolism for microbial chemical production. Nature 555 (7698), 683–687. https://doi.org/10.1038/nature26141.